Proceedings of the 3rd International Conference on Functional Materials and Civil Engineering
DOI: 10.54254/2755-2721/2025.GL29879

Experimental Research on Deployable Bridge

Chenyang Li[1†], Junyin Dai[2†], Mingxi Liu[3*†], Sunghee Kim[4†]

[1]*Jinan Xinhang Experimental Foreign Language School, Jinan, China*
[2]*Zhenhai High School of Zhejiang, Ningbo, China*
[3]*Oxford International College, Brighton, United Kingdom*
[4]*Chongqing Depu Foreign Language School, Chongqing, China*
**Corresponding Author. Email: Louis.mingxi.liu@outlook.com*
[†]*These authors contributed equally to this work and should be considered as co-first author.*

Abstract. This project explores the design of a compact deployable bridge that can be quickly assembled for rescue or temporary crossing. The structure combines a four-bar linkage frame on each side with a waterbomb origami deck, allowing the bridge to fold in two directions and stay stable after unfolding. The motion of the linkage was analysed using a complex-plane vector model to determine the relationship between link lengths and folding range. Based on this analysis, the geometry was optimised to reach a maximum span of 4.33 m while keeping the folded length below one-fifth of its deployed size. The waterbomb pattern was selected for the deck because it provides higher stiffness, smoother surface alignment, and better adaptability to uneven ground compared with single-direction folds. Several wooden prototypes were built to verify the motion sequence and connection details between the deck and frame. The final design can deploy continuously and lock automatically without extra fasteners. These results suggest that combining mechanical linkages with origami geometry offers a practical solution for lightweight bridges suitable for emergency rescue, military operations, and temporary field structures.

Keywords: deployable bridge, four-bar linkage, origami, waterbomb, kinematics, emergency rescue

1. Introduction

Bridges are essential for crossing rivers and ravines in both daily life and emergencies. Traditional fixed bridges, though stable, require long construction times, lack mobility, and often cannot meet the load demands of heavy rescue vehicles or equipment. To overcome these issues, folding bridges use compact, transportable structures that can be quickly deployed for earthquakes, floods, remote construction, or military operations.

Existing folding bridges fall into three main types: the Rolling Bridge in London, which rolls compactly but keeps its width, needs ground supports, and lacks self-locking; the Japanese Modular Foldable Bridge, which allows length adjustment with light modules but is slow to assemble, weak at joints, and bulky when folded; and the Hörn Bridge in Germany, which is simple and economical but has a fixed span, large storage width, and poor stability under adverse conditions [1].

DOI: 10.54254/2755-2721/2025.GL29879

Our design improves on these in four aspects: it folds bidirectionally to reduce stored volume to under one-fifth of its deployed size, allowing small-vehicle transport; it uses a four-bar side linkage that locks automatically when deployed for stability on uneven ground; geometric optimisation increases the single-unit span from 2.5 m to 4.33 m with potential for modular extension; and mirrored linkage design cancels height differences to keep the deck smooth and solve unevenness in modular bridges.

2. Design and analysis

2.1. Bridge side: design and analysis

2.1.1. Introduction

The frame delivers structural support and controlled deployment via two identical side four-bar linkages linked by a central parallelogram. Bar mechanisms like these have been widely studied for deployable structures because of their simple geometry and predictable motion [2]. A complex-plane model ensured smooth, branch-free motion and helps optimise the span within folded/deployed constraints, following the general principles of motion structures discussed by You and Chen [3].

2.1.2. Kinematic modelling

2.1.2.1. Modelling approach

We partition the mechanism into three loops (Fig. 1):

(1) left four-bar AB–AC–CD–DB; (2) central parallelogram CD–DF–EF–CE; (3) right four-bar GH–GE–EF–FH.

The left loop is expressed in vector form (Fig. 2) to derive the angular relationships used in subsequent optimisation.

To study the kinematics of the side four-bar linkages, the left mechanism is expressed in vector form (see Fig. 2). The vectors are defined as follows:

$$r_1 = BA, r_2 = AC, r_3 = CD, r_4 = DB \tag{1}$$

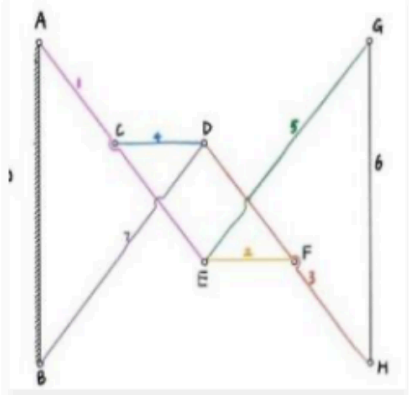

Figure 1. Side frame structure

DOI: 10.54254/2755-2721/2025.GL29879

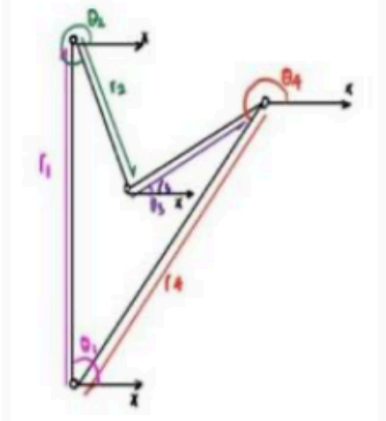

Figure 2. Closed-loop vector diagram of the left four-bar linkage

Expressing the four-bar loop in the complex plane, which provides a convenient way to derive the angular relationships and check the continuity of motion.

2.1.2.2. Kinematic modelling of the side four-bar linkage

Following the vector-equation method for planar linkages proposed by Guan [4], the loop closure of the four-bar can be written in the complex plane as

$$r_1 e^{\frac{\pi i}{2}} + r_2 e^{i\theta_2} + r_3 e^{i\theta_3} + r_4 e^{i\theta_4} = 0 \tag{2}$$

Separating real and imaginary parts gives two scalar equations:

$$Im : r_2 cos\theta_2 + r_3 cos\theta_3 + r_4 cos\theta_4 = 0,\ Re : r_1 + r_2 sin\theta_2 + r_3 sin\theta_3 + r_4 sin\theta_4 = 0. \tag{3}$$

By eliminating θ_3, the relation reduces to a first-order trigonometric form:

$$A\sin\theta_2 + B\cos\theta_2 + C = 0, \tag{4}$$

with coefficients

$$A = r_2(r_1 + r_4 sin\theta_4), B = r_2 r_4 cos\theta_4,\ C = \frac{1}{2}(r_1^2 + r_2^2 + r_4^2 - r_3^2) + r_1 r_4 sin\theta_4 \tag{5}$$

The input angle θ_2 can then be obtained in closed form as

$$\theta_2 = -\arctan2\,(B,A) + \arctan2\left(-C, \pm\sqrt{A^2+B^2-C^2}\right) \tag{6}$$

A valid solution exists when $|C| \le \sqrt{A^2+B^2}$. The two possible signs correspond to the two configuration branches of the four-bar. Once θ_2 is determined, the output angle θ_3 can be recovered from the closure equations using an atan2 form to preserve the correct quadrant.

DOI: 10.54254/2755-2721/2025.GL29879

2.1.3. Constraints

2.1.3.1. Folded state — minimal footprint

In the fully folded configuration, all four links AB, AC, CD, BD must be collinear so that every member lies on AB and does not extend beyond A or B. The necessary and sufficient conditions for collinearity are:

$$0^\circ \leq \angle ACD \leq 180^\circ \tag{7}$$

$$AB - AC + CD - BD = 0 \tag{8}$$

(these follow by setting all orientation angles in the original vector equation to 90° or 270°).Because $CD \| EF$, collinearity of AB, AC, CD, BD implies EF is also collinear; consequently, DH is collinear as well. Thus, all relevant members overlap along AB in the folded state. To ensure no element protrudes beyond AB, the following must also hold:

$$DH \leq BD \leq AB \tag{9}$$

$$AC \leq AE \leq AB \tag{10}$$

When conditions (7)-(10) are satisfied simultaneously, the mechanism attains its minimal folded footprint.

2.1.3.2. Deployed state — horizontal working configuration

Kinematic analysis in 2.2 shows no configuration keeps point H strictly horizontal to B throughout motion. For practical use, the working (deployed) state is defined when HB are horizontally aligned (i.e., deck fully unfolded). Span is evaluated only in this state, and the maximised span in 2.3 refers to this configuration.

2.1.3.3. Thickness & folding correction

If the deck thickness is a and there are b folds, the minimum folded thickness is approximated as ab. After optimisation, this value is rechecked to ensure the minimal-footprint requirement in 2.1.2 is met.

2.2. Bridge deck mechanism and improvement

1. Points B and H are at different heights during the opening process, as shown in Figure 3. Calculations below prove that adjusting the lengths of AB, BD, AC and CD cannot resolve this problem (assuming AB = GH, BD = DH = AE = EG and AC = CD = EF = FH)

DOI: 10.54254/2755-2721/2025.GL29879

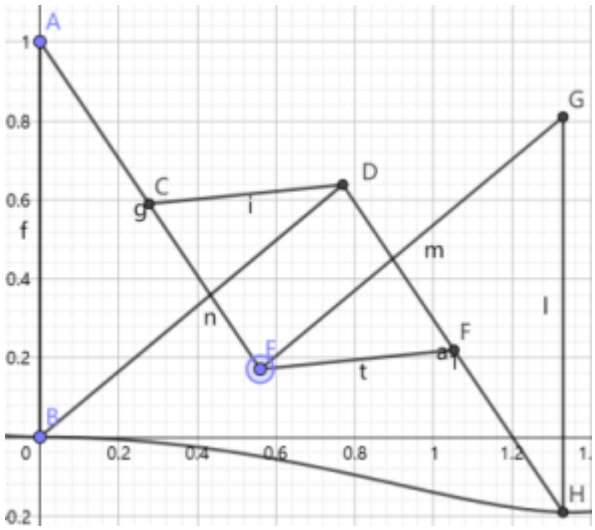

Figure 3. Difference of horizontal level between point B and H

$$Let\ BD = GE = AE = HD = 1,\ \angle DBH = \angle DHB = \angle EAG = \angle EGA$$

$$\mathrm{DE}\|\mathrm{AB}\|\mathrm{GH},\ \angle\mathrm{EAB}=\angle\mathrm{DBA}=\angle\mathrm{EGH}=\angle\mathrm{DHG}=\theta$$

$$\text{Let } \mathrm{AB}=\mathrm{GH}=\mathrm{a},\ \mathrm{AC}=\mathrm{HF}=\mathrm{k}. \tag{11}$$

Objective: Find k and a such that length CD is constant. Set coordinate system with point B at $(0,0)$, BA along positive x-axis, and BH along positive y-axis. Then the coordinates are:

$$D = (sin\theta, cos\theta),\ C = (ksin\theta, a - kcos\theta) \tag{12}$$

Define function $\mathrm{f}(\theta,\mathrm{k})$ as the square of length CD:

$$\mathrm{f}(\theta,\mathrm{k})=\mathrm{CD}^2=(1\text{-}\mathrm{k})^2(\sin\theta)^2+[\mathrm{a}\text{-}(1+\mathrm{k})\cos\theta]^2 \tag{13}$$

Suppose there is some k such that the length of CD won't change when θ changes. Then for such k, we have:

$$\frac{\partial \mathrm{f}}{\partial\theta}=2(1\text{-}\mathrm{k})^2\sin\theta\cos\theta+2[\mathrm{a}\text{-}(1+\mathrm{k})\cos\theta](1+\mathrm{k})\sin\theta=0 \tag{14}$$

Simplifying gives:

$$[(1\text{-}\mathrm{k})^2\text{-}(1+\mathrm{k})^2]\cos\theta+\mathrm{a}(1+\mathrm{k})=0 \tag{15}$$

Conclusion: There is no solution for k and a that can be expressed without θ.

Solution one is mirrored the two complete units to offset the height difference, as shown in figure 4.

DOI: 10.54254/2755-2721/2025.GL29879

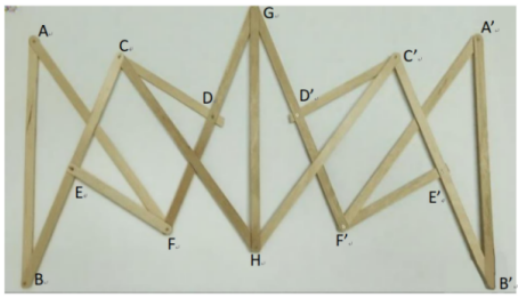

Figure 4. Mirrored the two units to offset the height difference

Solution two is by taking the values of the linkages and only use the range of motion where the track of H is close to a straight line. For instance, when AB = BD , AC = CD = 0.365 AB and select the range between x = 0.00 to x = 1.00, as shown in figure 5.

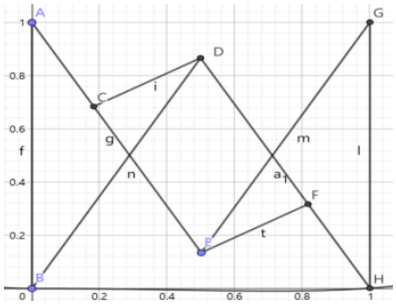

Figure 5. Choose the section with nearly straight track

2. If multiple units are connected together to make the bridge become longer, a single unit action cannot drive other units.

To solving this problem, we need add linkage mechanism to synchronise structural movements. For example, for the mirrored units case, by adding two revolute joint on FG and GF' and a sliding joint on GH with linkages connected between them, the movement of unit ABHG can drive the movement of unit HGA'B', as shown in figure 6.

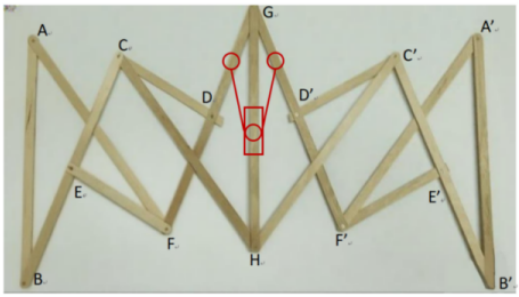

Figure 6. Add a linkage mechanism to synchronise structural movements

2.3. Optimisation strategy

2.3.1. Objective definition

Target variable: maximise the deck span BH in the deployed state. Constraints: conditions (1)–(4) from Section 2.1.3.1(folded state), the working-configuration definition from Section 2.1.3.2

DOI: 10.54254/2755-2721/2025.GL29879

(horizontal alignment of H and B), and the finite-thickness correction from Section 2.1.2.3 Fixed parameter: the ground link is set as AB = 2.5m

2.3.2. Geometric reasoning

When conditions (1)–(4) are satisfied, point D moves along a trajectory defined by the side four-bar linkage. Analysis shows that the deck span BH increases monotonically with the displacement of D, until D lies on the circular arc centred at A. At this limiting position, the triangle $\triangle ABH$ satisfies: $\angle AHB=30^\circ$

which yields the maximum deck span: $BH_{max}=\frac{AB}{\tan 30^\circ}$

2.3.3. Numerical result

For the case $AB=2.5\,m$: $BH_{max}=\frac{AB}{\tan 30^\circ}\approx 4.33m$

The corresponding link dimensions are: $AC=CD=1.25\,m$, $AB=BD=DH=2.5\,m$

This configuration meets all folded-state (collinearity and no overhang) and horizontal deployed-state (H and B aligned) constraints, while delivering the maximum usable span.

2.3.4. Thickness verification

Including the finite thickness a and fold number b, the folded width increases to approximately ab. Although this enlarges the physical thickness in storage, the deployed span BH_{max} remains unaffected. Thus, the optimised link dimensions are still valid in practice, provided the folded thickness does not exceed allowable design limits.

2.3.5. Proof of maximum span

Geometric proof of maximum span

Let a circle be drawn with centre B and radius AB. This circle defines the feasible region for point D.

Proof by contradiction: Assume that the maximum span BH can be achieved when D lies strictly inside the circle. Take an interior point D_1. Draw a horizontal line through D_1 intersecting the circle at D_0. From D_1, drop the vertical to point H, and construct $D_{0H_0}\|D_1H$, such that H_0 lies on the x-axis at the same height as H.

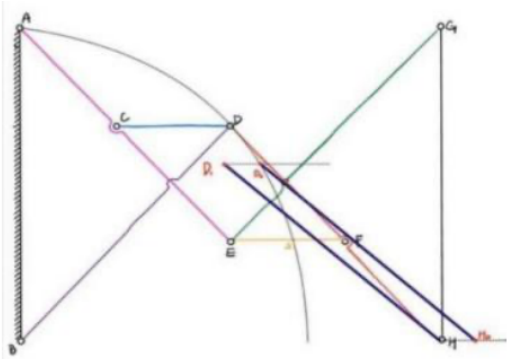

Figure 7. Geometric construction for the proof of maximum span

DOI: 10.54254/2755-2721/2025.GL29879

By construction, $BD_1<BD_0, D_1H=D_0H_0$, which implies $BH<BH_0$. This contradicts the assumption that D_1 could give the maximum span. Therefore, point D must lie on the circular arc to achieve the maximum span. Furthermore, when D is on the arc, it is clear that the span BH is maximised when DH itself is maximised. In this limiting case, the link lengths satisfy $AB = BD = DH$. Once D lies on the arc, it is clear that BH is maximised when DH itself is maximised. In this case, the link lengths satisfy $AB = BD = DH$.

Substituting this into condition (2) from Section 2.1.2 gives $AC = CD$. Finally, as D moves from left to right along the arc, the value of BH increases monotonically. The limiting configuration occurs when points A, C, D, and H become collinear, consistent with condition (1). This extreme position corresponds to the deployed state with the maximum span.

2.4. Results

2.4.1. Angular relationship between θ2 and θ4

Figure 7 illustrates the relationship between the input angle θ_2 and the output angle θ_4 for the side four-bar linkage when $r_1=r_4=2.5\,m$, $r_2=r_3=1.25\,m$.

The curve demonstrates a smooth and monotonic variation of θ_2 with respect to θ_4, confirming that the mechanism operates continuously without binding or branch switching. This validates that the folded configuration can be smoothly transformed into the deployed configuration under the given dimensions.

2.4.2. Parametric span analysis

To verify the optimisation, the side link lengths were varied by setting $r_2=r_3=x$,

with x ranging between 0 and 2.5 m, while keeping $r_1=r_4=2.5m$. For each value of x, the span in the horizontal deployed configuration was calculated. Figure 8 shows the resulting span–parameter curve. The span increases with x, reaches a clear maximum at $x=1.25\,m=0.5\,AB$, and then decreases symmetrically. This confirms that the optimal condition derived in Section 2.3 —namely AC=CD=1.25 m—indeed provides the maximum span.

It should be noted, however, that the feasible domain of x is restricted. Numerical evaluation shows that a valid horizontally deployed state only exists when $0.36\,AB\leq x\leq 0.5\,AB$.

For $x < 0.36\,AB$, the locus of point H remains strictly above the x-axis and never intersects it. For $x > 0.5\,AB$, the locus lies entirely below the x-axis and again never intersects it.

Therefore, the practical range of x for which the mechanism can actually deploy to a horizontal configuration is limited to this interval. Figure 9 – Span BH as a function of x when $r_2=r_3=x$, with $AB=2.5\,m$. The maximum is reached at $x=1.25\,m$.

2.4.3. Summary of findings

The kinematic relationship in Figure 8 confirms that the mechanism deploys smoothly for the selected link lengths. The parametric study in Figure 9 verifies that the maximum usable span occurs at x=1.25 m, consistent with the geometric proof.

At this optimum, the link configuration is $AC=CD=1.25\,m$, $AB=BD=DH=2.5\,m$, yielding the maximum deck span $BH_{max}\approx 4.33\,m$.

DOI: 10.54254/2755-2721/2025.GL29879

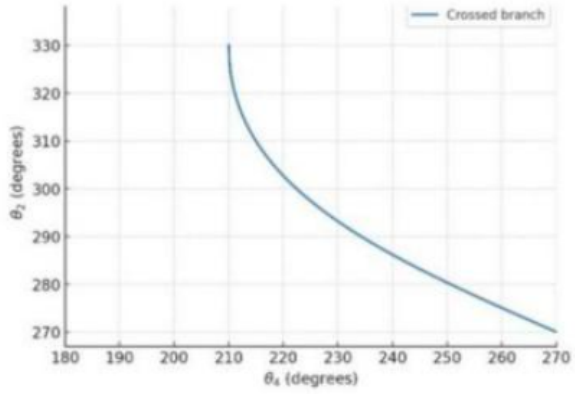

Figure 8. Angle continuity of the mechanism: θ_2 vs θ_4

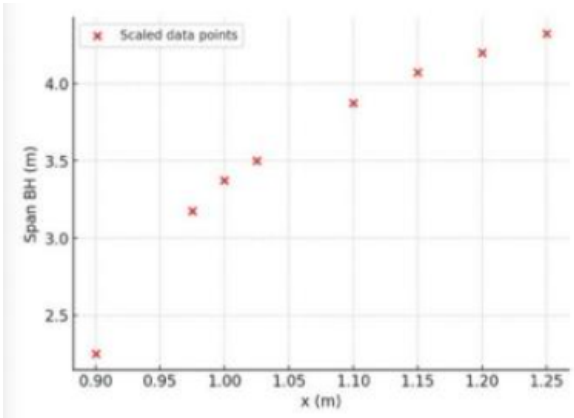

Figure 9. Span BH as a function of x

2.5. Bridge deck design and analysis

2.5.1. Bridge deck structure

The initial design was to fold the paper in half, as shown in Figure 10.

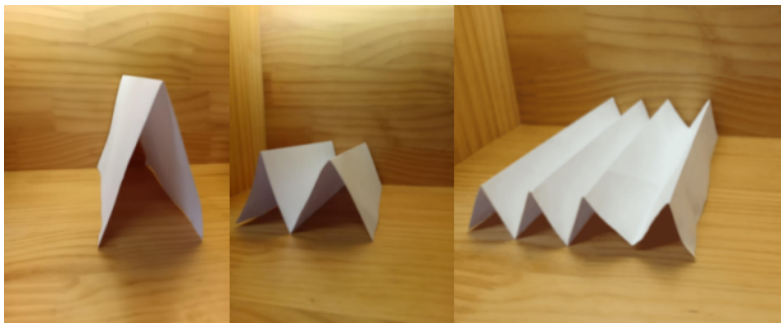

Figure 10. Fold the paper in half or more times

Initial folding instability and wind susceptibility when partially unfolded were addressed by proposing a boat-shaped structural design, which was specifically optimised as a hollow triangular box shape, enhancing the bending resistance of the bridge deck(figure 11).

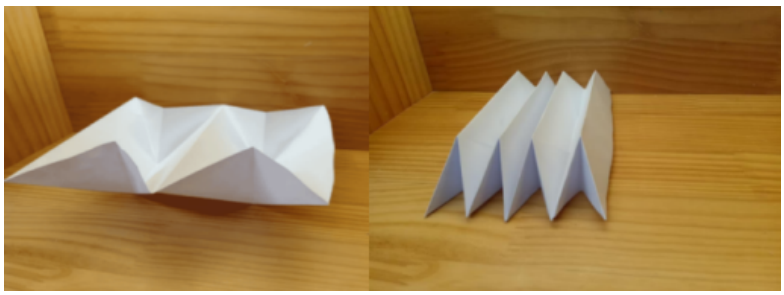

Figure 11. Fold the paper boat shape and for more times

But this structure only folds in one direction, which deviates from our goal of quick and convenient improvement. Inspired by other origami prototypes such as the FRC Origami Bridge

DOI: 10.54254/2755-2721/2025.GL29879

Model [5] and Origami Antennas [6], finally, we have finally decided to design the bridge deck as the water bomb structure. As shown in Figure 12, finally, we have decided to design the bridge deck as the water bomb structure. As shown in Figure 12.

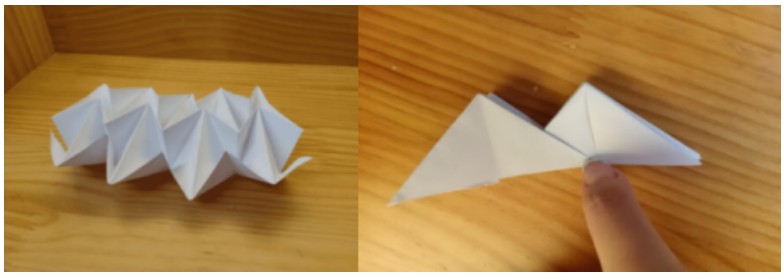

Figure 12. Fold the paper in a waterbomb structure

It can achieve bidirectional folding, with a smaller folding volume and the ability to twist and stabilise in multiple directions. This allows it to adapt to non-parallel terrain, further improving the practicality of our bridge. As shown in Figure 13.

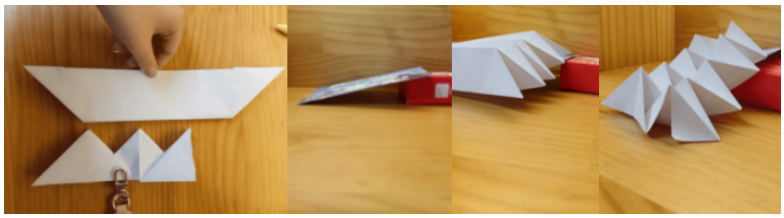

Figure 13. Higher degree of folding and adaptability of the waterbomb structure

2.5.2. Further design of waterbomb structure

The case of edges that are with A and Bare different(figure 14).

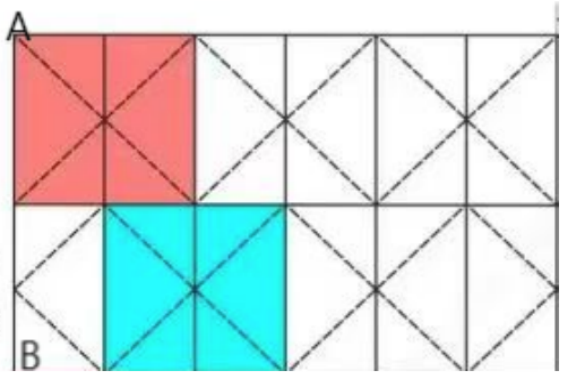

Figure 14. Waterbomb's two edges

In a detailed analysis, if the edge is case A, when it is folded, the two adjacent sides of A overlap, forming a groove. At this point, angle A is 45 degrees when folded (figure 15).

DOI: 10.54254/2755-2721/2025.GL29879

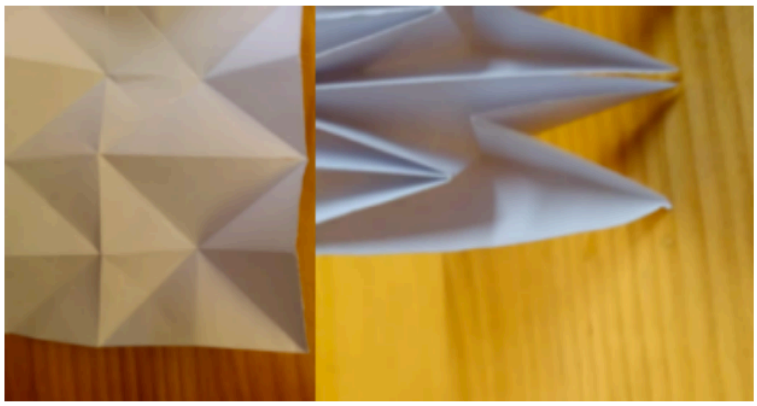

Figure 15. Waterbomb edge with case A

As for case B, when it folded, the B point folded inside, and the angle of point B is 90° (figure 16). Causing a change in its position in horizontally when folded, which makes it difficult to connection between the bridge deck and the bridge side, making it a poor design.

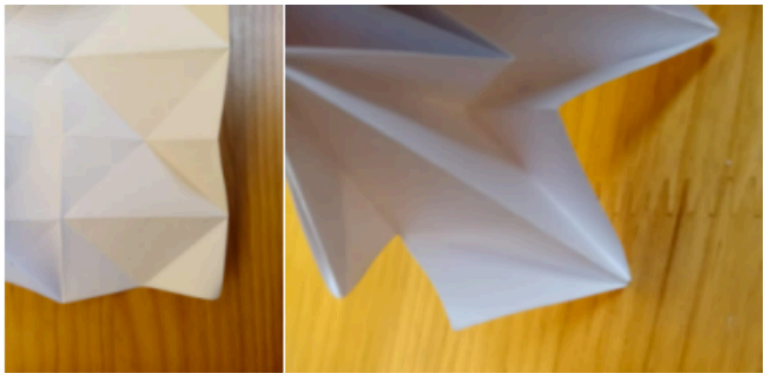

Figure 16. Waterbomb edge with case B

Besides, apart from case A and case B, another design cuts half of the units on the edges as shown in Figure 17. In this case, the angle formed when folded changes from 45°to 90°.

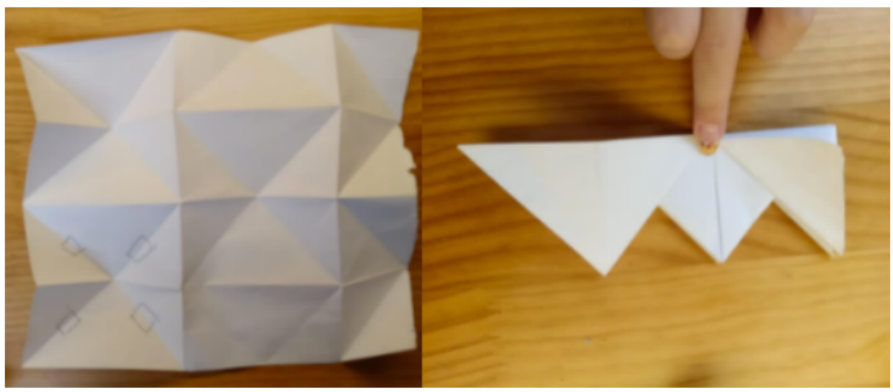

Figure 17. Comparison between edges with a complete unit and a half-unit waterbomb

DOI: 10.54254/2755-2721/2025.GL29879

3. Construction of prototypes

3.1. Prototype of bridge side

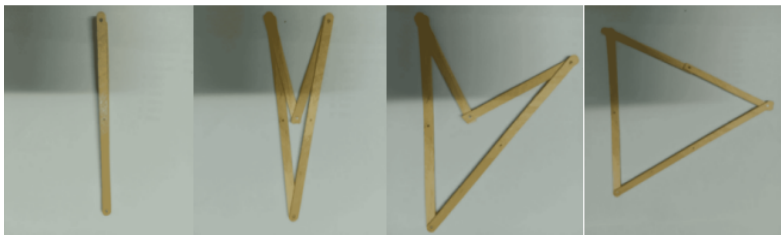

Figure 18. The opening process of a four-bar linkage in one unit

Figure 18 shows the opening process of one four-bar linkage in one unit.

The initial prototype constructed with straws has a relatively large thickness, hindering precision due to our 2D design. To improve the precision, we switch to wooden strips 1 mm thick and smaller nails (figure 19).

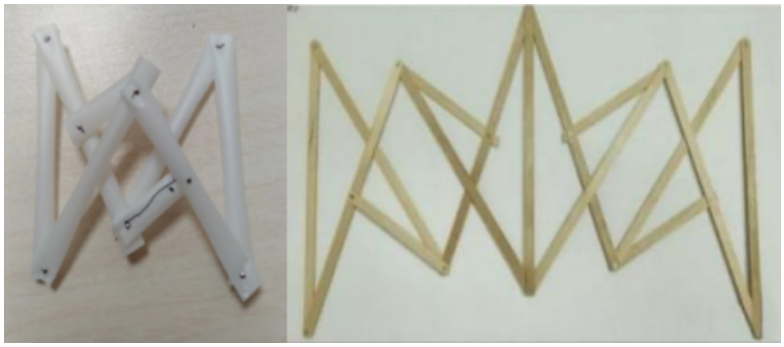

Figure 19. Switch of the prototype between a straw and a wooden strip

3.2. Prototype of bridge deck

Due to the original design, where the points were connected, the connection surface was too small and not stable enough. To enhance stability, we redesigned the deck by cutting off a section to enlarge the small contact surface(Figure 20).

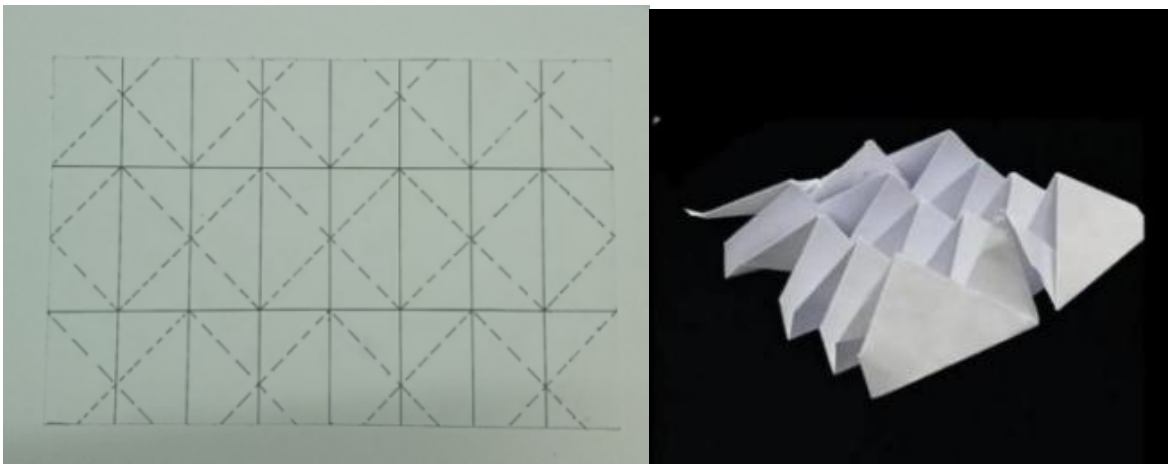

Figure 20. Redesign of bridge deck

DOI: 10.54254/2755-2721/2025.GL29879

3.3. Connection between the bridge deck and the bridge frame and final prototype

The final design requires joints between the deck and frames. The connections must ensure the overall stability and safety in real-life conditions, while allowing both the deck and the frame to fold completely.

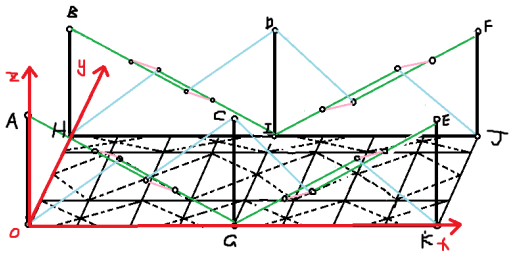

Figure 21. Final design figure

Figure 22. Connection between deck and frame

Point connections at vertices (e.g., point O, H in Fig. 21) make the bridge weak and unsafe under load. We strengthened the system by changing point connections to line of connections (Fig. 22). A hollow tube was attached along the deck edge and the metal rods with a joint connected to the bridge railings passed through, improving stability while preserving foldability. The overall deployment process of the bridge is illustrated step-by-step in Fig. 23, showing how the structure unfolds smoothly from a compact folded state to the fully deployed configuration.

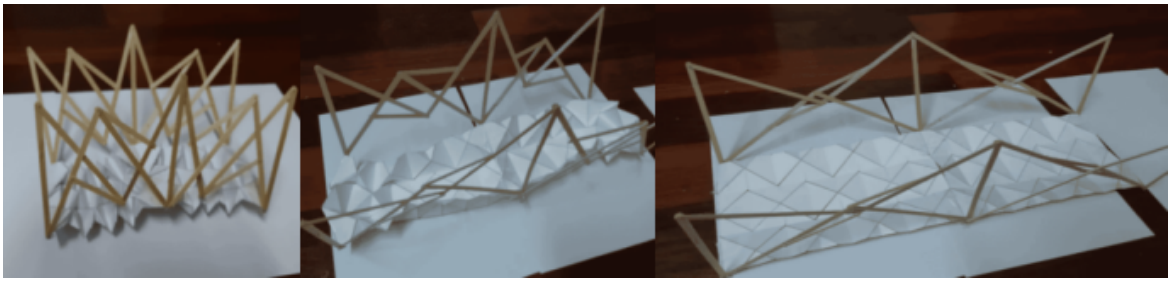

Figure 23. The entire process of the bridge unfolding

4. Conclusion

4.1. Evaluation of the deployable bridge

4.1.1. Advantages of deployable bridge

Compared with the previously mentioned deployable bridge cases, our deployable bridge features a larger folding-unfolding ratio. As shown in Figure 24, traditional bridges that fold only along the x-axis (often increasing height along y), while our design folds along both x and y axes without a significant increase in z-height, thanks to the waterbomb origami deck. Our designed foldable bridge with a larger folding-unfolding ratio will have greater advantages in other scenarios, such as emergency rescue.

DOI: 10.54254/2755-2721/2025.GL29879

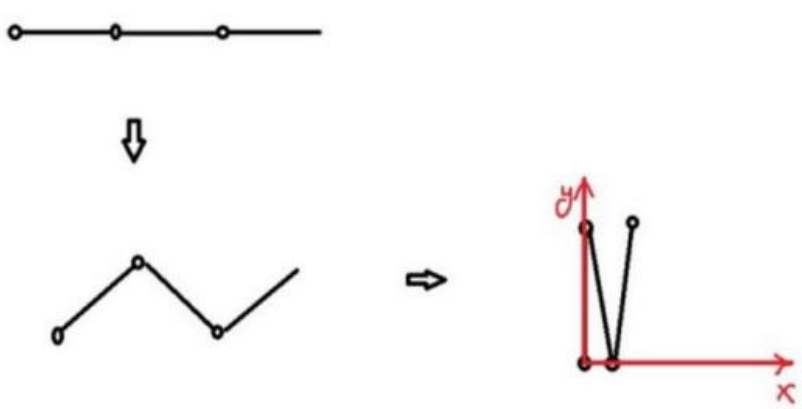

Figure 24. Traditional bridge frame

In addition, our deployable bridge exhibits excellent stability. Primarily, we chose this link mechanism as the side frame due to its retractable and deployable movement mode, and its ability to automatically lock in place when fully unfolded. preventing sliding further forward. This ensures the deployable bridge does not slide or retract when loads are moved on the deck, thereby enhancing the bridge's stability, reliability, and safety in practical application scenarios.

4.1.2. Stability and potential issues

When there is a load on the deck, the deployable bridge risks collapsing inward because there are no other connections between the two sides of the bridge except the deck itself. To address this problem, we connect point A to point B and point C to point D. (figure 25).In this way, we can obtain a bridge structure with a triangular cross-section. Due to the stability of the triangle, when the deck is fully unfolded, the deck and the frameworks on both sides will support each other, thereby preventing collapse.

Since the triangular structure limits the height of the bridge, we derive a geometric model to calculate the maximum size of the truck that can just pass through the bridge.(figure 26). we let HO=x, AR=y, PQ=h, PM=w. Then, we can obtain the equation: $w \times h = (x - h)(y - h)$

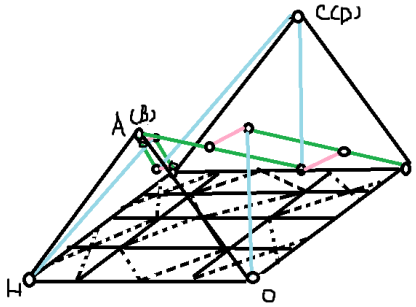

Figure 25. Unit 3D structural diagram

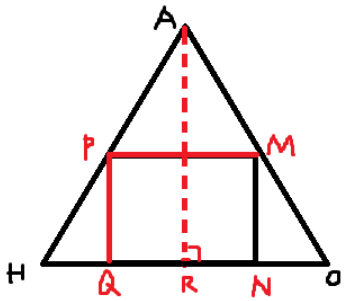

Figure 26. Cross-sectional area diagram

DOI: 10.54254/2755-2721/2025.GL29879

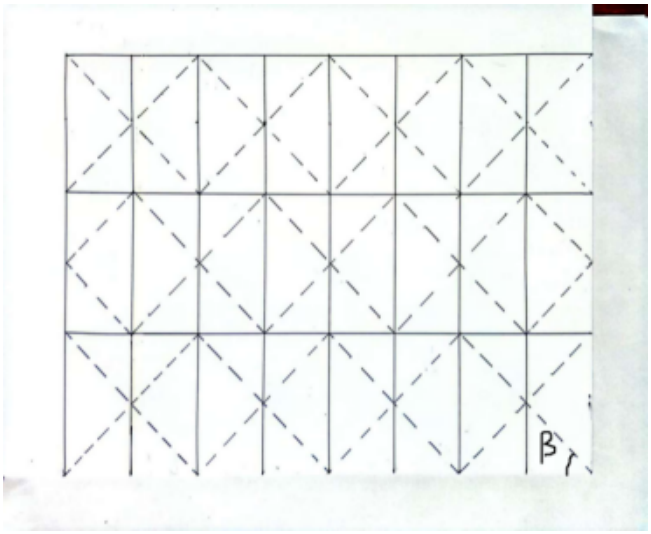

Figure 27. Origami deck pattern diagram

Besides, the folding pattern of the waterbomb should also be modified to adapt to this change. When the bridge is folded, OH will become shorter. With ∠AOH=α and β=45°,(figure 27), the structure can fold smoothly without jamming

4.2. Conclusion of design

In conclusion, we designed a deployable bridge combining a linkage side frame with a waterbomb origami deck, which fills the gap of scarce practical cases in this field since it can fold in two directions, lock automatically when unfolded, and keep the deck smooth and stable. This design improves upon previous single-direction folding bridges by offering greater compactness and portability. Kinematic analysis and physical prototypes demonstrate its larger span, foldability and its structural stability. Our bridge can be applied in various fields, including emergency rescue, military operations, post-disaster reconstruction and field research, and similar self-powered monitoring systems for deployable bridges have recently been explored [7]. While further testing and improvement on material and load-capacity testing are still in desperate need for real-world implementations.

Author contribution statement

This article was co-authored by Chenyang Li, Junyin Dai, Mingxi Liu, and Sunghee Kim, all of whom share equal contribution as co-first authors. The order of authors is arranged alphabetically by first name.

References

[1] Ario, I., Nakazawa, M., Tanaka, Y., Tanikura, I. and Ono, S. (2013). Development of a prototype deployable bridge based on origami skill. Automation in Construction, 32, pp.104–111. doi: https://doi.org/10.1016/j.autcon.2013.01.012

[2] Doroftei, I.A., Bujoreanu, C. and Doroftei, I. (2019). Structural and kinematic aspects of some bar mechanisms for deployable structures. IOP Conference Series: Materials Science and Engineering, 591, 012077. doi: https://doi.org/10.1088/1757-899X/591/1/012077

[3] You, Z. and Chen, Y. (2011). Motion Structures. CRC Press.

DOI: 10.54254/2755-2721/2025.GL29879

[4] Guan, L. (1997). Vector equation analysis method for planar four-bar linkage mechanism. Journal of Nanchang University (Engineering & Technology), 19(2), pp.29–32.
[5] Salák, M. and Frantová, M. (2019). FRC Origami Bridge Model. IOP Conference Series: Materials Science and Engineering, 596, p.012038. doi: https: //doi.org/10.1088/1757-899x/596/1/012038
[6] Georgakopoulos, S.V., Zekios, C.L., Sattar-Kaddour, A., Hamza, M., Biswas, A., Clark, B., Ynchausti, C., Howell, L.L., Magleby, S.P. and Lang, R.J. (2021). Origami Antennas. IEEE Open Journal of Antennas and Propagation, 2, pp.1020–1043. doi: https: //doi.org/10.1109/ojap.2021.3121102
[7] Xia, K., Liu, J., Li, W., Jiao, P., He, Z., Wei, Y., Qu, F., Xu, Z., Wang, L., Ren, X., Wu, B. and Hong, Y. (2023). A self-powered Bridge Health Monitoring System Driven by Elastic Origami Triboelectric